The Astrophysical Journal, 759:87 (5pp), 2012 November 10 doi:10.1088/0004-637X/759/2/87

ENERGY DEPOSITION PROFILES AND ENTROPY IN GALAXY CLUSTERS

Anya Chaudhuri[1], Biman B. Nath[2], and Subhabrata Majumdar[1]
[1] Tata Institute of Fundamental Research 1, Homi Bhabha Road, Mumbai 400005, India; anya@tifr.res.in, subha@tifr.res.in
[2] Raman Research Institute, Sadashiva Nagar, Bangalore 560080, India; biman@rri.res.in
Received 2012 April 11; accepted 2012 August 22; published 2012 October 22

ABSTRACT

We report the results of our study of fractional entropy enhancement in the intracluster medium (ICM) of the clusters from the representative *XMM-Newton* cluster structure survey. We compare the observed entropy profile of these clusters with that expected for the ICM without any feedback, as well as with the introduction of preheating and cooling. We make the first estimate of the total, as well as radial, non-gravitational energy deposition up to r_{500} for this large, nearly flux-limited, sample of clusters. We find that the total energy deposition corresponding to the entropy enhancement is proportional to the cluster temperature (and hence cluster mass). The energy deposition per particle scaled by $T_{\rm sp}$, $\Delta E/T_{\rm sp}$ has a similar profile in all clusters, and is more pronounced in the central regions. Our results support models of entropy enhancement through active galactic nucleus feedback.

Key words: galaxies: clusters: general – X-rays: galaxies: clusters

Online-only material: color figures

1. INTRODUCTION

Models of structure formation in the universe have been successful in predicting the global properties of galaxy clusters. These characteristics, such as gas temperature, X-ray luminosity, Sunyaev–Zel'dovich flux, and richness, make it possible to draw cosmological conclusions from surveys of galaxy clusters (e.g., Reiprich & Böhringer 2002; Vikhlinin et al. 2009; Gladders et al. 2007; Khedekar et al. 2010; Rozo et al. 2010; Sehgal et al. 2011; Benson et al. 2011). The detailed properties of the intracluster medium (ICM) however are described by baryonic physics in addition to the dark matter potential in which it resides (e.g., Shaw et al. 2010; Battaglia et al. 2011; Trac et al. 2011; Chaudhuri & Majumdar 2011). It is believed that feedback from galaxies, including active galactic nuclei (AGNs), and/or radiative cooling of the ICM gas, modifies the X-ray properties of the gas (see McNamara & Nulsen 2007, 2012). These non-gravitational processes tend to increase the entropy of the ICM gas, thereby making it tenuous, and consequently, underluminous in X-rays, especially in low temperature (and mass) clusters.

Recent observations of profiles of entropy (defined as $K = k_B T/n_e^{2/3}$, where n_e is the electron number density and k_B is the Boltzmann constant[3]) allow one to compare them with theoretically expected profiles with or without feedback, and allow one to determine the nature and degree of feedback. Entropy as defined above is well suited for this sort of analysis as it is a record of the accretion of gas into the cluster, as well as the modifications shaped by the processes of gas cooling and feedback. Voit et al. (2005) had shown that in the absence of any feedback and cooling processes, simulations tend to predict a power-law radial profile for the entropy outside the core, with a scaling $K \propto r^{1.1}$.

Since entropy per particle is a Lagrangian quantity, it is more sensible to study the distribution of entropy not with the radial distance, but with the gas mass, taking into account the movement of gas shells due to a change in entropy. Voit et al. (2005) suggested the comparison of entropy as a function of gas mass in order to determine the enhancement of entropy from non-gravitational processes (see also Nath & Majumdar 2011). Here, we study the entropy profiles of clusters from the representative *XMM-Newton* cluster structure survey (REXCESS) sample and compare these with the baseline profiles of the ICM without any feedback. For these clusters, Pratt et al. (2010) studied the radial entropy profiles, and after comparing them with the initial profile, found that entropy enhancement is evident in the inner radii, and that it extends up to large radii for low mass systems, while large mass clusters do not show entropy deviation at very large radii. Here, we focus on the entropy profiles as functions of gas mass. We determine TdK/K, where dK/K is the fractional deviation of the observed entropy from the benchmark theoretically calculated entropy, which is a measure of the energy deposition per particle, and investigate the profile of this energy deposition for low and high temperature clusters.

We adopt a ΛCDM cosmology with $H_0 = 70$ km s^{-1} Mpc^{-1}, $\Omega_M = 0.3$, and $\Omega_\Lambda = 0.7$.

2. THE CLUSTER SAMPLE

The REXCESS survey (Böhringer et al. 2007) uses the REFLEX cluster catalog as a parent sample. REFLEX is a nearly complete flux-limited cluster sample, covering 4.24 sr in the southern extragalactic sky (Böhringer et al. 2004). This sample consists of 31 local clusters in the redshift range $z \leqslant 0.2$, where the clusters are selected on the basis of their X-ray luminosity, $L_X = (0.407\text{–}20) \times 10^{44}\ h_{50}^{-2}$ erg s^{-1} in the 0.1–2.4 keV band, with a homogeneous coverage in the chosen luminosity range, and no preference for any morphology type. The selected luminosity range provides clusters with a temperature $\gtrsim 2$ keV and does not include galaxy groups. As Pratt et al. (2010) have noted, the properties of the REXCESS sample allow one to study the variation of entropy profiles across a range of cluster masses, especially because the distances were chosen such that r_{500} fell within the *XMM-Newton* field of view, which increased the precision of measurements at large radii. They also subdivided the sample into cool-core and non-cool-core systems, defining

[3] We write K for the entropy popularly defined in X-ray literature, and denote the thermodynamic entropy as S.

the clusters with central density $E(z)^{-2}n_{e,0} > 4\times10^{-2}$ cm^{-3} as cool-core systems ($E(z)$ being the ratio of the Hubble constant at redshift z to its present value).

In this work, we use the entropy profiles of 25 clusters from the whole REXCESS sample of 31 clusters (see Pratt et al. 2010, their Table 1). We use only those clusters with data at a minimum of five radial points outside the core radii, thus excluding cluster numbers 2, 13, 23, 25, and 27 (ordered top to bottom, respectively, in the table). We also leave out cluster number 14, whose errors on observed entropy far exceed those of other clusters.

3. ENTROPY PROFILES

3.1. Initial Entropy—Radial Profile

In order to assess the entropy enhancement in observed clusters, we first discuss the profile expected without any non-gravitational processes. Voit et al. (2005) presented an analytic form for the baseline entropy profile which they obtained by analyzing the entropy profiles of clusters from non-radiative simulations. Their simulated smoothed particle hydrodynamics profiles, when fitted in the 0.1–1 r_{200} range, scatter about a median-scaled profile described by a baseline power-law relation,

$$\frac{K(r)}{K_{200}} = 1.32\left(\frac{r}{r_{200}}\right)^{1.1}, \quad (1)$$

with approximately 20% dispersion.

3.2. Initial Entropy Profile with Gas Mass

In this paper, we would like to study the entropy as a function of gas mass. In order to calculate the initial entropy profile as a function of gas mass, we use the initial radial entropy profile, in conjunction with the assumption of hydrostatic equilibrium. We assume the Navarro–Frenk–White profile for the dark matter halo (Navarro et al. 1997). For the concentration parameter $c_{500} = 3.2$ that we adopt,[4] the corresponding relation for Equation (1) at r_{500} becomes (Pratt et al. 2010)

$$\frac{K(r)}{K_{500}} = 1.42\left(\frac{r}{r_{500}}\right)^{1.1}. \quad (2)$$

The equation of hydrostatic equilibrium can be written as

$$\frac{dP_g}{dr} = -\rho_g\frac{GM(<r)}{r^2} = -\left[\frac{P_g}{K}\right]^{3/5} m_p\mu_e^{2/5}\mu^{3/5}\frac{GM(<r)}{r^2}, \quad (3)$$

where $P_g = n_g k_B T$ is the gas pressure. For the boundary condition, the total gas fraction inside $r_{\rm vir}$ is set to the universal baryon fraction, $f_g = \Omega_b/\Omega_m$. Equations (2) and (3) are solved for the pressure profile P_g from which we determine the entropy profile $K_{\rm th}(M_g)$.

The resulting profile $K_{\rm th}(M_g)$ scaled by K_{500}, the characteristic entropy (Equation (3) in Pratt et al. 2010), is shown in Figure 1 (upper panel), for clusters in different temperature bins. We have fitted the profile with the form, $K_{\rm th}(M_g)/K_{500} = A\,(M_g/M_{500})^{\alpha}$, in the range $0.1r_{200}$–r_{500}. For the whole sample of clusters, the slope $\alpha = 0.81\pm0.05$ and the normalization $A = 6.09\pm0.86$, where the small scatter reflects the near self-similarity of the $K_{\rm th}(M_g)/K_{500}$ profiles in the figure.

[4] This value is measured for a morphologically relaxed cluster sample by Pointecouteau et al. (2005), also used by Pratt et al. (2010).

Table 1
Mean Values of Parameters in the Range $0.1r_{200}$–r_{500} (Excluding Core): Observed Entropy–Gas-mass Relation

Sample	A_o	B_o	α_o
Total sample (25 clusters)	0.23 ± 0.43	9.59 ± 7.54	0.67 ± 0.47
Cool-core (9)	0.14 ± 0.61	9.07 ± 6.18	0.63 ± 0.61
Non-cool-core	0.28 ± 0.30	9.89 ± 8.38	0.69 ± 0.40

3.3. Observed Entropy—Radial Profile

Pratt et al. (2010) have fitted the REXCESS data to the form

$$K(r) = K_0 + K_{100}[r/100\ {\rm kpc}]^{\alpha}, \quad (4)$$

where K_0 is interpreted as the excess of core entropy above the best-fitting power law at large radii. They scaled the quantities to r_{500}, the effective limiting radius for high-quality observations from *XMM-Newton* and *Chandra*. Interior to r_{500}, the observed entropy is always higher than the baseline prediction. At r_{500}, they find that the median dimensionless entropy is $K(r_{500})/K_{500} = 1.70\pm.35$ and that this is higher than, but consistent with, the baseline prediction.

3.4. Observed Entropy Profiles with Gas Mass

Next, we express the observed entropy profiles $K_{\rm obs}/K_{500}$ of REXCESS clusters as a function of M_g/M_{500}. Figure 1 (lower panel) shows these profiles for all 25 clusters in our sample in different temperature ranges. We fit each individual profile by an expression of the form $K_{\rm obs}/K_{500} = A_o + B_o\,(M_g/M_{500})^{\alpha_o}$, in the range $0.1r_{200}$–r_{500}. The mean and scatter of the parameters A_o, B_o, and α_o for all the clusters is shown in Table 1. Since the scatter is large, a single fit to the entire sample is not done. Here, the mean values stated are simply the mean of the parameters for all the clusters and is not a fit to the entire cluster sample. Nevertheless, note that the power-law indices for the observed entropy–gas-mass relation are shallower than those for the theoretical relation. Interestingly, this index (logarithmic slope) does not differ much in the whole cluster sample. The values of A_o and B_o show that cool-core clusters are entropy deficient.

4. EFFECTS OF ONLY PREHEATING AND COOLING

Voit et al. (2002) discussed three types of modifications to the initial entropy profile: (1) a truncation in the entropy profile owing to removal of gas, approximating the effect of gas cooling and dropping out of the ICM; (2) a shift in the profile, mimicking the effect of preheating; and (3) lowering the entropy profile due to radiative cooling. Assuming a form of the cooling function of the type $\Lambda \propto T^{-1/2}$ for group temperatures ($T \leqslant 2$ keV), it was shown that $K^{3/2}$ across the cluster is reduced by an amount $3/2K_c^{3/2}$, where K_c is a critical entropy. Johnson et al. (2009) suggested a combination of the effects of preheating and cooling, expressed as

$$K_{\rm obs}^{3/2} = (K_{\rm th} + K_{\rm shift})^{3/2} - \frac{3}{2}K_c^{3/2}, \quad (5)$$

where $K_c \approx 81\,{\rm keV\,cm^2}[T/1\,{\rm keV}]^{2/3}\,[t/14\,{\rm Gyr}]^{2/3}$ (their Equation (14)) describes the cooling. They calculated the constant preheating shift $K_{\rm shift}$ by evaluating Equation (5) at their outermost radial point.

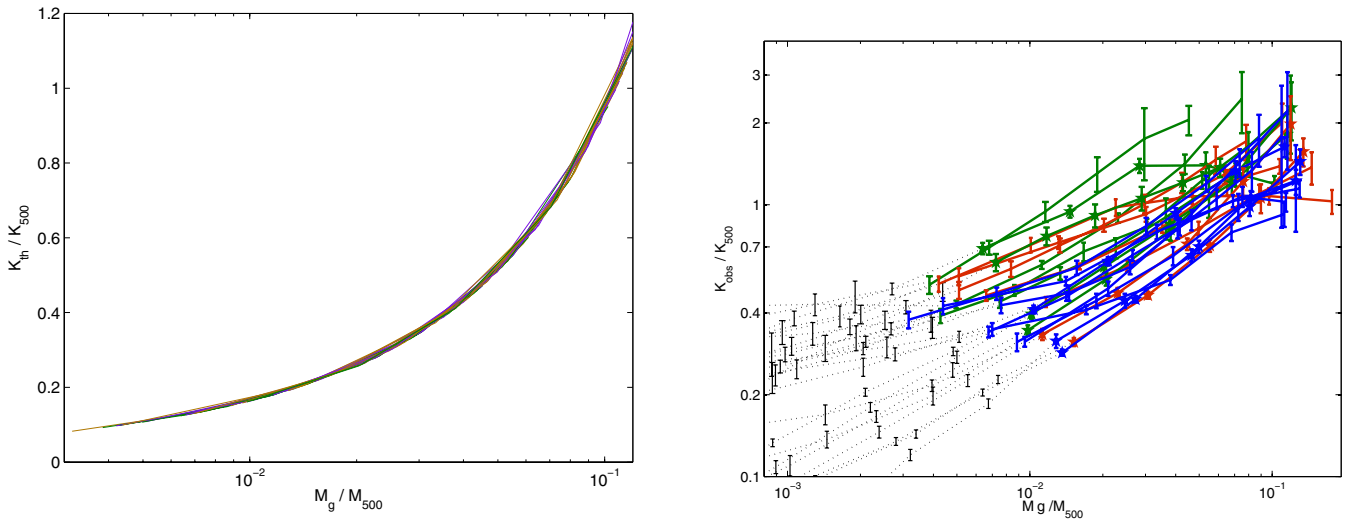

Figure 1. Upper panel: this plot shows the ratio of $K_{\rm th}/K_{500}$ as a function of gas mass M_g for all the clusters. Green lines refer to the lowest temperature clusters ($T_{\rm sp} \leqslant 3.5$ keV), red for the intermediate temperature clusters (3.5keV $\leqslant T_{\rm sp} \leqslant$ 5 keV), and blue lines are for the largest temperature clusters ($T_{\rm sp} \geqslant 5$ keV). Lower panel: $K_{\rm obs}/K_{500}$ is plotted against M_g/M_{500}. Color scheme is the same as above. Dotted lines show observations below $0.1r_{200}$. $T_{\rm sp}$ is the mean spectroscopic temperature in the 0.15–0.75 r_{500} range (Pratt et al. 2010).

(A color version of this figure is available in the online journal.)

For the 28 nearby galaxy groups from the *XMM-Newton* survey, Johnson et al. (2009) found that while this "preheating + cooling" model matches the observations better than a simple shift/truncation, it still fell short of being a reasonable representation of the observed profiles.

We have fitted models of the form of Equation (5) to our sample, where we have used the entire profile $K_{\rm th}(M_g)$ and $K_{\rm obs}(M_g)$, rather than just one radial point for the fit. We attempted three different types of fits for each cluster, described below: (1) K_C is evaluated using the full radial temperature profile instead of mean temperature; (2) a fit using the constant $T_{\rm sp}$ for each cluster; (3) we assume that a fraction of the gas mass is lost from the ICM, and try two fits with varying fractions of the total gas mass, $f = 0.8, 0.9$. The temperature $T = T_{\rm sp}$, and the expression used for the fitting is $K_{\rm obs}(f\ M_g) = [(K_{\rm th}(M_g) + K_{\rm shift})^{3/2} - (3/2)K_C^{3/2}]^{2/3}$.

We find that the number of clusters for which none of the fits are good far exceeds the clusters for which any of the fits can be called reasonable (reduced $\chi^2 < 2$). The lack of a good fit to the preheating+cooling model in most of the clusters in the sample suggests that a major component of entropy enhancement occurs beyond simple preheating and radiative cooling.

Cooling is however essential to explain the condensation of ~15% of ICM into stars. Condensation and galaxy formation preceding cluster formation can help to explain the entropy excess (e.g., Voit et al. 2003).

5. FRACTIONAL ENTROPY DEVIATION AND ENERGY INPUT

In order to determine the amount of energy deposition associated with the entropy enhancement, we use the quantity $T_{\rm obs}\Delta K/K_{\rm obs}$, where $\Delta K = K_{\rm obs} - K_{\rm th}$. This is because the thermodynamic entropy of an ideal gas S is related to K, as $S = \text{const.} \times \ln K$ and the change in energy per unit mass $dQ = TdS \propto T\Delta K/K$ (see also Equation (3) of Finoguenov et al. 2008).

In an isochoric process (see also Lloyd-Davies et al. 2000),

$$\Delta Q = \frac{\Delta K n_e^{2/3}}{(\gamma-1)\mu {\rm m}_p} = \frac{kT_{\rm obs}}{(\gamma-1)\mu {\rm m}_p}\frac{\Delta K}{K_{\rm obs}}. \quad (6)$$

In an isobaric process, however (for $T_f/T_i = \beta$),

$$\Delta Q = \frac{\Delta K n_f^{2/3}}{\left(1-\frac{1}{\gamma}\right)\mu {\rm m}_p}\frac{\beta^{2/3}(\beta-1)}{(\beta^{5/3}-1)} = \frac{kT_{\rm obs}}{\left(1-\frac{1}{\gamma}\right)\mu {\rm m}_p}\frac{\beta^{2/3}(\beta-1)}{(\beta^{5/3}-1)}\frac{\Delta K}{K_{\rm obs}}. \quad (7)$$

The ratio of the changes in energy for a given fractional change $\Delta K/K_{\rm obs}$ and $T_{\rm obs}$ is given by

$$\frac{\Delta Q_{\rm isobaric}}{\Delta Q_{\rm isochoric}} = \gamma\frac{\beta^{2/3}(\beta-1)}{(\beta^{5/3}-1)}. \quad (8)$$

For a value of $\beta = (2, 0.5)$, the above ratio is $(1.21, 0.77)$. This implies that if the observed temperature $T_{\rm obs}(M_g)$ deviates from the theoretically calculated value $T_{\rm th}(M_g)$ by a factor $\leqslant$2, then the two above-mentioned estimates of energy input per unit mass differ by ~20%. Figure 2 shows the ratio $T_{\rm th}(M_g)/T_{\rm obs}(M_g)$ for clusters in the sample. One can see that the two temperature profiles vary within a factor of ~2; hence, we choose the expression for the isochoric process in our estimate. Note that the final $T_{\rm obs}$ may differ from the gas temperature, T_2, right after feedback due to adiabatic cooling. Thus, $\beta > 2$ since, now, $T_{\rm th}/T_2 < 2$. The right-hand side of Equation (8) will approach γ in the limit of large β.

We first estimate the energy per particle, $\Delta E(M_g) = 3/2\ T_{\rm obs}(\Delta K/K_{\rm obs})$, for each cluster. Figure 3 shows the profiles for $\Delta E/T_{\rm sp}$, the ratio of the non-gravitational energy injection to the gravitational potential of the clusters in three temperature bins. While the detailed profiles differ from cluster to cluster, $\Delta E/T_{\rm sp}$ generally has a decreasing profile with a similar trend. Albeit with a large scatter within each temperature group, we

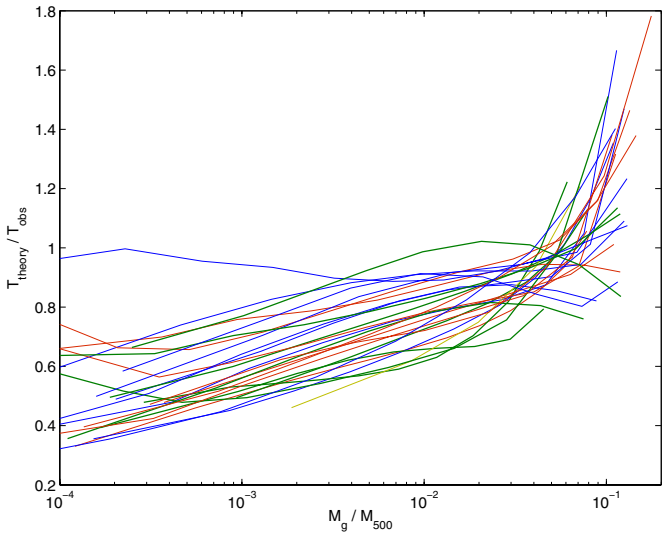

Figure 2. Ratio of the theoretical to observed temperature as a function of M_g/M_{500} is plotted for our sample of 25 clusters.

(A color version of this figure is available in the online journal.)

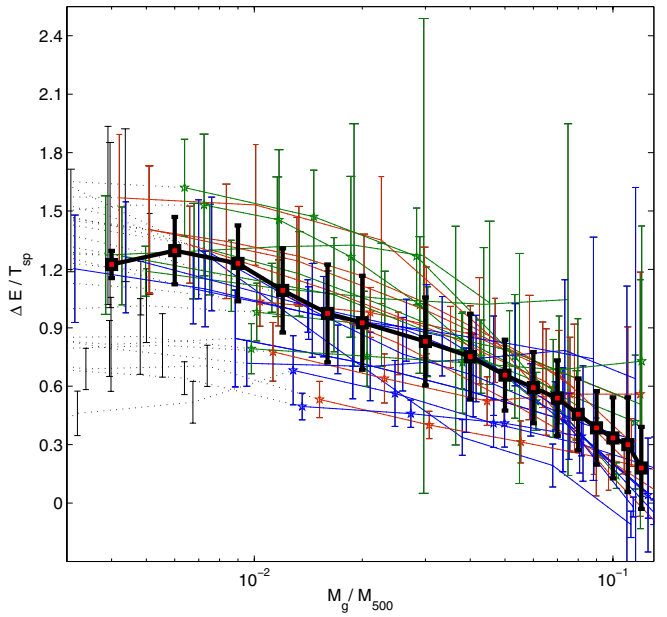

Figure 3. Profiles of energy deposition per unit particle plotted against M_g/M_{500}, after scaling them by T_{sp} for different clusters. Data points inside the core radii are shown in dotted lines. The color scheme is the same as that used in Figure 1. The mean profile and 1σ scatter, outside the core radii, is shown with the thick black line.

(A color version of this figure is available in the online journal.)

find that the mean value of $\Delta E/T_{sp}$ is higher for the low temperature group. For all clusters, non-gravitational energy is already comparable to the gravitational energy at the core radii. Moreover, the profiles decrease by 50% for $T_{sp} \leqslant 3.5$ keV clusters and 75% for $T_{sp} > 3.5$ keV clusters. Thus, on average, the profiles for higher masses decrease faster than those for lower masses. Our calculations as mentioned earlier are valid outside the core,.1 R_{200}.

We determine the mean profile after averaging over all the ΔE profile fits for the individual clusters.[5] The mean profile with

[5] To this end, we use the fit $\Delta E = C + D\,(M_g/M_{500})^{\delta}$.

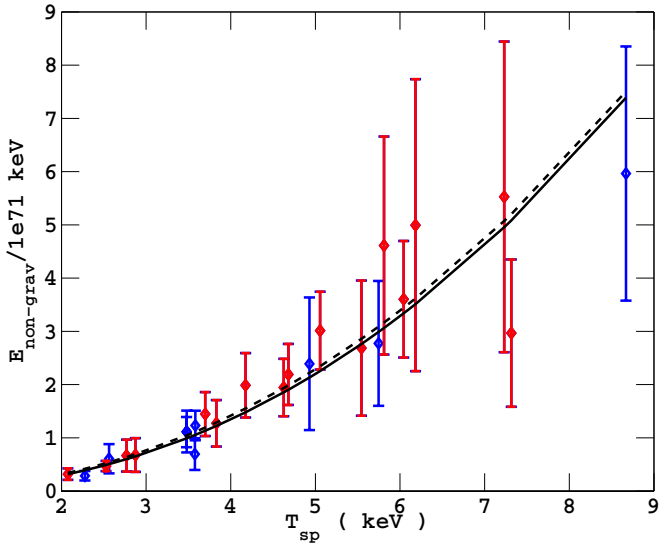

Figure 4. Total energy injection between $0.1r_{200}$–r_{500} is plotted against cluster mass. Red points are for non-cool-core clusters and blue points show cool-core clusters. The best fit to entire sample is shown in the solid black line. The black dashed line shows best fit to the non-cool-core clusters.

(A color version of this figure is available in the online journal.)

the 1σ scatter is shown in Figure 3. The mean profile decreases by roughly a factor of four between $0.1r_{200}$ and r_{500}.

The total amount of energy deposited for the whole cluster is

$$E_{\text{non-grav}} = \int \frac{kT_{\text{obs}}}{(\gamma-1)\mu m_p}\frac{\Delta K}{K_{\text{obs}}}\,dM_g\,, \qquad (9)$$

for M_g/M_{500} between the limits $0.1r_{200} < r < r_{500}$. We use the fits obtained above to calculate the integral and the results are shown in Figure 4. Clearly, $E_{\text{non-grav}}$ is proportional to the cluster mass. A fit results in the following scaling relations for the whole sample:

$$\frac{E_{\text{non-grav}}}{10^{71}\,\text{keV}} = (1.35 \pm 0.091)\left(\frac{T_{\text{sp}}}{4\,\text{keV}}\right)^{2.20\pm0.17}. \qquad (10)$$

If the cool-core clusters are omitted, then one obtains a slope of $2.16 \pm .21$ and a normalization of $1.41 \pm .12$.

Dividing the energy by the total number of particles in the ICM, we estimate the mean energy to be 2.74 ± 0.87 keV per particle.

6. DISCUSSIONS

We note that the error bars on our results (e.g., the error on the scaling parameters (e.g., Equation (10)) are large. These reflect mainly the large error bars on the data points, T_{obs} and S_{obs}. Better data from future observations will tighten these results.

Earlier observations of entropy enhancement, mostly inferred from the deviations of several cluster scaling relations, were interpreted in terms of an entropy floor. For example, preheating simulations by Borgani et al. (2001) showed that an entropy floor of $\sim$50 keV cm^2, roughly corresponding to $\sim$1 keV per particle, was adequate to explain the observations.

From a sample of *Chandra* clusters, Mathews & Guo (2011) have compared potential energy derived from the observed density profiles to those from an "initial" adiabatic density profile to estimate energy deposition. Our entropy-based calculation naturally incorporates *both* density and temperature profiles in the

estimation of energy deposition. They find a mean energy feedback of 3.6(4.8) keV per particle for clusters with mean mass $M_{500} = 3.1 \times 10^{14}\, M_{\odot}(7.6 \times 10^{14}\, M_{\odot})$ when averaged up to the "adiabatic" virial radius. Unlike them, we have confined our results to R_{500} and have not extrapolated beyond the maximal observed radii.

Interestingly, Roychowdhury et al. (2004) showed for their model of AGN feedback from black holes that X-ray observations could be explained with an energy input proportional to cluster mass. In their model of AGN feedback through buoyant bubbles of relativistic plasma, which deposit energy into the ICM through pdV work, convection and thermal conduction, this proportionality implied a linear relation between the black hole mass of the central AGN and the cluster mass. We find that in order to explain the correlation in Figure 4, we need the black hole mass $M_{\rm bh} \sim 2 \times 10^{-6} M_{500}\eta_{0.2}$, where the energy available from the AGN is characterized by an efficiency $\eta = 0.2$. Recent simulations by Gaspari et al. (2012) also show the energy deposition to be centrally peaked.

We have estimated the energy input corresponding to the entropy enhancement differently from previous works. First, we have not used any cluster scaling relations which depend on the average properties of the ICM. We have also used the distribution of the X-ray entropy (K) with gas mass, since entropy per unit mass (S) is a Lagrangian quantity. Furthermore, instead of determining an entropy floor and then estimating an amount of energy assuming a certain density, we have estimated the energy input from first principles.

Our result implies that the effect of energy deposition in low and high temperature clusters is remarkably similar. The similarity in the profiles can provide a test for future simulations. Second, the gas mass profiles of energy deposition per particle show that the processes responsible for entropy enhancement in clusters affect the gas in the central regions more than in the outer regions.

Taken together, our results indicate that the energy associated with entropy enhancement is proportional to cluster mass. Furthermore, their effect in all clusters is centrally peaked. This suggests an energy source which must satisfy both requirements simultaneously. As mentioned earlier, AGN feedback models satisfy these requirements (Roychowdhury et al. 2004; Gaspari et al. 2012).

7. SUMMARY

We have looked at the fractional entropy enhancement in the ICM for a sample of REXCESS clusters by comparing the observed entropy profiles to those expected from gravitational collapse only. We first show that this entropy excess cannot be explained by only preheating plus cooling models of entropy enhancement. Since this entropy excess must be sourced from non-gravitational processes, we connect this excess to any non-gravitational energy deposition in the ICM. We report, to our knowledge, the first energy deposition profiles in a large sample of clusters and also estimate the total non-gravitational energy that has been dumped into the ICM. We find that this excess energy is proportional to cluster temperature (and hence cluster mass). We show that the entropy enhancement process in the ICM is centrally peaked and is larger in low temperature clusters than in high temperature clusters. Our results support models of entropy enhancement through AGN feedback.

The authors thank the referee for constructive comments and Gabriel Pratt for providing the data on which this work is based. A.C. thanks RRI for hospitality.

REFERENCES

Battaglia, N., Bond, J. R., Pfrommer, C., & Sievers, J. L. 2011, arXiv:1109.3711
Benson, B. A., de Haan, T., Dudley, J. P., et al. 2011, arXiv:1112.5435
Böhringer, H., Schuecker, P., Guzzo, L., et al. 2004, A&A, 425, 367
Böhringer, H., Schuecker, P., Pratt, G. W., et al. 2007, A&A, 469, 363
Borgani, S., Governato, F., Wadsley, J., et al. 2001, ApJ, 559, L71
Chaudhuri, A., & Majumdar, S. 2011, ApJ, 728, L41
Finoguenov, A., Ruszkowski, M., Jones, C., et al. 2008, ApJ, 686, 911
Gaspari, M., Ruszkowski, M., & Sharma, P. 2012, ApJ, 746, 94
Gladders, M D., Yee, H. K. C., Majumdar, S., et al. 2007, ApJ, 655, 128
Johnson, R., Ponman, T. J., & Finoguenov, A. 2009, MNRAS, 395, 1287
Khedekar, S., Majumdar, S., & Das, S. 2010, Phys. Rev. D, 82, 041301
Lloyd-Davies, E. J., Ponman, T. J., & Cannon, D. B. 2000, MNRAS, 315, 689
Mathews, W. G., & Guo, F. 2011, ApJ, 738, 155
McNamara, B. R., & Nulsen, P. E. J. 2007, ARA&A, 45, 117
McNamara, B. R., & Nulsen, P. E. J. 2012, New J. Phys., 14, 055023
Nath, B. B., & Majumdar, S. 2011, MNRAS, 416, 279
Navarro, J. F., Frenk, C. S., & White, S. D. M. 1997, ApJ, 490, 493
Pointecouteau, E., Aranaud, M., & Pratt, G. W. 2005, A&A, 435, 1
Pratt, G. W., Arnaud, M., Piffaretti, R., et al. 2010, A&A, 511, A85
Reiprich, T., & Böhringer, H. 2002, ApJ, 567, 716
Roychowdhury, S., Ruszkowski, M., Nath, B. B., & Begelman, M. C. 2004, ApJ, 615, 681
Rozo, E., Wechsler, R. H., Rykoff, E. S., et al. 2010, ApJ, 708, 645
Sehgal, N., Trac, H., Acquaviva, V., et al. 2011, ApJ, 732, 44
Shaw, L. D., Nagai, D., Bhattacharya, S., & Lau, E. T. 2010, ApJ, 725, 1452
Trac, H., Bode, P., & Ostriker, J. P. 2011, ApJ, 727, 94
Vikhlinin, A., Kravtsov, A. V., Burenin, R. A., et al. 2009, ApJ, 692, 1060
Voit, G. M., Balogh, M. L., Bower, R. G., Lacey, C. G., & Bryan, G. L. 2003, ApJ, 593, 272
Voit, G. M., Bryan, G. L., Balogh, M. L., & Bower, R. G. 2002, ApJ, 596, 601
Voit, G. M., Kay, S. T., & Bryan, G. L. 2005, MNRAS, 364, 909